

FRED: Flexible REduction-Distribution Interconnect and Communication Implementation for Wafer-Scale Distributed Training of DNN Models

Saeed Rashidi^{*§}, William Won^{*}, Sudarshan Srinivasan[‡], Puneet Gupta[†], and Tushar Krishna^{*}

^{*}Georgia Institute of Technology, Atlanta, USA

[†]UCLA, Los Angeles, USA

[‡]Intel, Bangalore, India

saeed.rashidi@gatech.edu, william.won@gatech.edu, sudarshan.srinivasan@intel.com
puneetg@ucla.edu, tushar@ece.gatech.edu

arXiv:2406.19580v1 [cs.AR] 28 Jun 2024

Abstract—Distributed Deep Neural Network (DNN) training is a technique to reduce the training overhead by distributing the training tasks into multiple accelerators, according to a parallelization strategy. However, high-performance compute and interconnects are needed for maximum speed-up and linear scaling of the system. Wafer-scale systems are a promising technology that allows for tightly integrating high-end accelerators with high-speed wafer-scale interconnects, making it an attractive platform for distributed training. However, the wafer-scale interconnect should offer high performance and flexibility for various parallelization strategies to enable maximum optimizations for compute and memory usage. In this paper, we propose FRED, a wafer-scale interconnect that is tailored for the high-BW requirements of wafer-scale networks and can efficiently execute communication patterns of different parallelization strategies. Furthermore, FRED supports in-switch collective communication execution that reduces the network traffic by $\approx 2\times$. Our results show that FRED can improve the average end-to-end training time of ResNet-152, Transformer-17B, GPT-3, and Transformer-1T by $1.76\times$, $1.87\times$, $1.34\times$ and $1.4\times$ respectively, when compared to a baseline waferscale 2D-Mesh fabric.

I. INTRODUCTION

Deep Neural Networks (DNNs) models are on an exponential growth curve. A recent study shows that in less than two years, the compute and memory requirements for DNN training have increased by $1800\times$ and $1500\times$, respectively [39]. Distributing the training across multiple accelerators or Neural Processing Units (NPU) is a common practice today to reduce the training time. However, one critical side-effect of distributed training is the communication overhead between NPUs to synchronize model gradients and/or activations, depending on the *parallelization strategy*. As the number of NPUs scale, the communication overhead increases, up to a point where it becomes the dominant factor in distributed training latency [35], [34], [17], [18].

There are fundamental limits to the bandwidths that can be provided even by high-speed rack-scale fabrics (such as NVlinks [22]) and thus there has been a growing interest towards platforms that integrate multiple NPUs together on the

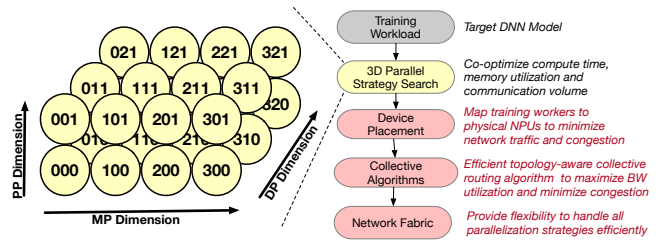


Fig. 1. HW-SW Co-Design Stack for Optimizing DNN Training Communication. This work addresses the three phases highlighted in red. The left part of the figure shows a sample logical view of training workers in 3D-parallelism. The parallelization strategy is of size MP(4)-DP(3)-PP(2), meaning that there are 4/3/2 peer workers for MP/DP/PP dimension. Each worker is named with 3 digits, representing the id of worker in the MP, DP, and PP dimension, respectively. Workers that are aligned along each dimension, should *communicate* for that respective dimension’s parallelization type. For example, workers 000, 100, 200, and 300 should communicate for MP type (i.e., activation/input gradient sync during forward-pass/back-propagation), while workers 300, 310, 320 should communicate for DP type (weight gradient sync during the back-propagation)

same package. Cerebras demonstrated one extreme incarnation of this idea in the form of a monolithic wafer with NPUs connected to one another. More cost- and yield-effective waferscale approaches involve integrating NPU chiplets and DRAM chiplets together [32], [26], [33]. While there is broad agreement on the scalability and bandwidth benefits that wafer-scale substrates can provide, the architecture of the on-wafer fabric connecting the NPUs remains an open question. All wafer-scale accelerator proposals to date (e.g., Cerebras CS2 [1], Tesla Dojo [26], Tensorrent Wormhole [33], UCLA’s waferscale GPU [32]) have implemented a 2D mesh topology. The choice of a mesh is understandable. It is the most pervasive topology in many-core chips given its ease of place-and-route and scalability, and is the natural choice on a many-chiplet substrate as well. However, this work demonstrates that the inherent blocking nature of the mesh topology is extremely inefficient for DNN training communication use cases.

To design an optimal fabric for DNNs, it is crucial to first understand the communication needs. Communication in DNN

[§]The work was done when the author was a PhD student at Georgia Tech in 2022.

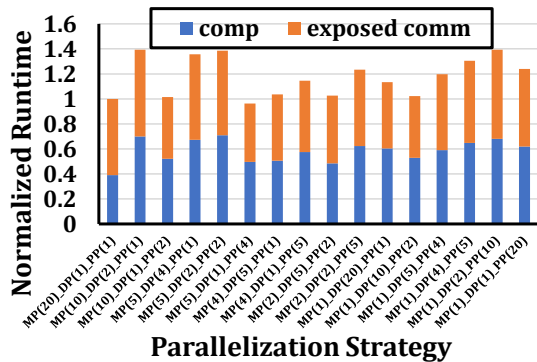


Fig. 2. The normalized comp/comm overhead for various parallelization strategies (explained in Sec. II) of Transformer-17B, when running on top of the 2-D mesh topology (as described in Sec. VI) that connects 20 NPUs on the wafer.

training depends inherently on the parallelism strategy being employed. Data-Parallel (DP) [23], [18], Model-Parallel (MP) [21], [17], and Pipeline-Parallel (PP) [16], [27], are the building blocks of any parallelism strategy. In DP, the DNN model is replicated across NPUs and each NPU works on different set of training samples (minibatch). In MP, each DNN layer is sharded across NPUs while they work on the same training samples. In PP, each NPU hosts a subset of DNN layers, and training samples flow through NPUs in a pipeline manner. 3D-parallelism [28] utilizes all aforementioned strategies by creating different MP/DP/PP groups between NPUs. The optimal balance between DP, MP and PP is heavily dependant on the workload and underlying platform and can *significantly vary for different workload/platform configurations* [17]. Fig. 1 shows an example of a 3D parallelism strategy (Sec. II provides more details).

From a communication perspective, 3D-parallelism requires executing *multiple concurrent communication operations* between NPUs within the same MP/DP/PP group at different stages of distributing training. Moreover, different parallelism strategies stress the compute and communication differently. This is quantified in Fig. 2. As the figure shows, high communication overhead can result in the total training overhead of compute-efficient strategies being greater than the less compute-efficient strategies (e.g., MP(20)-DP(1)-PP(1), vs. MP(5)-DP(4)-PP(1)). An inefficient network fabric can force the compiler to discard some parallelization strategies due to their poor communication performance on the fabric, effectively trading compute and memory performance for lower communication overhead. Additionally, an inefficient network complicates the device placement and communication primitive algorithms for a given parallelization strategy.

In summary, an optimal fabric for DNN training should meet the following three needs.

- 1) *Handle multiple non-blocking collective communications with minimum congestion*
- 2) *Efficient for all 3D-parallelism configurations*
- 3) *Provide high-BW connectivity between NPUs*

In this work, we propose *FRED*, a wafer-scale network fabric for supporting arbitrary 3D-parallelism. To address (1)

and (2), *FRED* includes: (a) a network fabric architecture comprising a novel topology with switches that provide native support for reduction and broadcast for bandwidth amplification, (b) a collective routing algorithm with non-blocking support, and (c) device placement algorithm to minimize congestion. Fig. 1 highlights these features. To address (3), we deploy *FRED* over a wafer-scale substrate [31]. Each “NPU” in our architecture is a hybrid integration of compute chiplets and 3D-stack DRAM chiplets. We also discuss solutions to layout and scale the *FRED* topology over the wafer.

To the best of our knowledge, *FRED is the first work that is tailored for high-BW of wafer-scale interconnects and can efficiently support concurrent in-network collectives of hybrid parallelization strategies (e.g., 3D-parallelism)*. Hence, *FRED* enables the compiler to consider any type of parallelization strategies without any concern about efficiently they can be executed on the network. In summary:

- We motivate the challenges with designing a wafer-scale fabric for 3D-parallelism (Sec. III).
- We propose *FRED*, a novel network fabric that includes several innovative features: **a switch fabric** with flexible reduction-distribution trees connected via a scalable topology (Sec. IV), **a novel routing algorithm** to route multiple collectives concurrently along with a congestion-aware device placement policy for 3D-parallelism (Sec. V).
- We demonstrate how *FRED* can be implemented as a wafer-scale fabric (Sec. VI).
- We compare *FRED* with baseline fabrics for some sample workloads and parallelization strategies (Sec. VIII). Our results show that *FRED* can improve the average end-to-end training time of ResNet-152, Transformer-17B, GPT-3, and Transformer-1T by 1.76 \times , 1.87 \times , 1.34 \times and 1.4 \times when compared to the baseline 2D-Mesh, respectively.

II. BACKGROUND

A. Collective Communication Patterns

Although DNN models can be highly diverse, most of their communication during distributed training can be handled through collective patterns [18]. Depending on the model type and parallelization strategy, different types of collectives may be needed to synchronize on activations/gradients during forward-pass/back-propagation [35]. Fig. 3 shows the mathematical implication of collective patterns between three workers. During *Reduce-Scatter*, workers should communicate together in such a way that at the end, each worker has a portion of globally reduced data. In *All-Gather*, each worker broadcast its local data to all other workers. *All-Reduce* is the most common pattern in distributed training [18] and can be thought of a *Reduce-Scatter* followed by an *All-Gather*. In *Reduce*, multiple NPUs participate in reducing data and the result is stored only on one NPU, while *Multicast* means a single NPU sends its data to multiple NPUs. In *All-to-All*, each worker sends a portion of its local data to each worker, as indicated in Fig. 3.

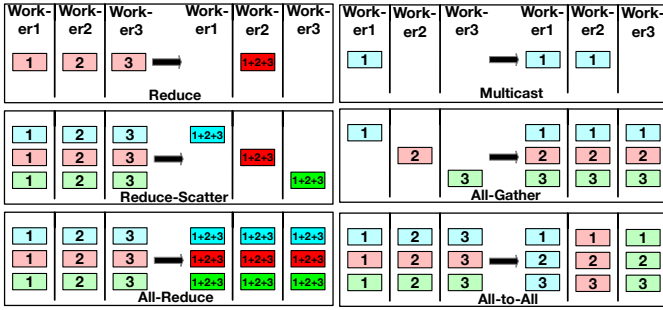


Fig. 3. Collective communication patterns between three workers.

B. Collective Communication Algorithms

The patterns described in Sec. II-A can be handled through different *collective algorithms*. NPUs communicate in a peer-to-peer distributed manner (without requiring central coordination). The optimal routing algorithm is usually dependent on the physical network topology and collective size. For example, ring-based All-Reduce is optimal when the physical topology is a ring, while tree-based All-Reduce is optimal for tree-based topologies, or when the message size is small [42]. One drawback of NPU-to-NPU based approach is the amount of traffic it generates. For example, the most BW optimal NPU-to-NPU algorithms require each NPU to send/receive nearly $\frac{2(N-1)}{N}D$ bytes data to execute an All-Reduce of D bytes among N NPUs [18]. To alleviate this, recent proposals have proposed in-network collective algorithms by adding the compute capability to the switches [37], [18], [24]. This lets the endpoint resources be allocated for training compute tasks, while the network switches handle the collectives. As a result, an All-Reduce of D bytes only requires each NPU to send/recv D bytes, reducing the traffic by half compared to the traditional approach.

C. Communication in 3D Parallelism

There are multiple ways of distributing the distributed training tasks across multiple NPUs (a.k.a. the parallelization strategy): MP [41], DP [23], and PP [16], [27]. The combination of these strategies can be generalized in the form of 3D-parallelism [28]. Fig. 1 shows the concept of 3D-parallelism. In this case, each training worker is a part of one MP, DP, and PP group, where the id (offset) of each NPU within its MP/DP/PP group is determined using the first/second/third digits of a 3-digit worker id. Therefore, the NPUs that have the same DP & PP digits are within the same MP group (e.g., 000, 100, 200, and 300). Similarly, we can obtain the workers within the same DP or PP group.

The NPUs within the same DP group should communicate through the *All-Reduce* collective pattern during the back-propagation to sync their locally computed model gradients and update the model before starting the next training iteration [18]. The pattern changes to *Reduce* for weight streaming (Sec. III-A). For the MP group case, NPUs need to communicate during forward-pass/back-propagation to synchronize on output-activations/input-gradients. The communication pattern, however, depends on the layer type and

the way it is sharded. The usual observed patterns are: *All-Reduce* [41], *All-to-All* [29], *Reduce-Scatter* [21], and *All-Gather* [21]. For the PP group, the NPUs need to transfer the output-activations/input-gradient during forward-pass/back-propagation on the borderline layers and pass the data to the NPU(s) hosting the next set of layers.

Fig. 1 also shows the necessity to handle multiple collectives at the same time. For e.g., there are eight different DP groups, meaning that up to eight concurrent All-Reduces should be handled for the DP communications (similarly there are six/twelve concurrent communication operations for MP/PP communications). Moreover, the communication type and peer workers differ across MP, DP, and PP groups. Thus, it is crucial for the underlying network fabric to be flexible for concurrent and different collective patterns.

D. Wafer-Scale Systems

Wafer-scale platforms offer a high-bandwidth and energy-efficient alternative to traditional package scaling [31]. In general, two methods have been proposed: (i) A monolithic integration where all NPUs and the interconnect are fabricated on the wafer substrate directly [1], [38]. (ii) Chiplet-based integration where NPUs are fabricated separately and then bonded to the wafer-scale interconnect (e.g., interposer or Silicon interconnect Fabric (Si-IF)) [40], [31]. In this approach, components from different technologies (e.g., DRAM) can be integrated on the wafer. Additionally, since the chiplets can be tested before integration, this approach has a better yield and requires less redundancy compared to the first approach. FRED is applicable to both integration methods. However, we use the integration (ii) and its associated HW parameters when evaluating our approach in Sec. VIII.

Baseline Wafer-Scale Topologies. Recent products and research in wafer-scale platforms are based on interconnecting NPUs through a 2D-mesh topology [32], [1], [31]. Among the main reasons for choosing 2D-mesh for wafer-scale platforms are ease of place & route and area optimality of it [32]. Thus, in this paper, we choose 2D-mesh as the main baseline topology and compare our proposal against it.

III. MOTIVATION

In this section, we tease out key design principles for architecting a fabric for wafer-scale platforms.

A. Execution Modes

Current wafer-scale systems have up to 40 GB on-chip SRAM memory [1]. While this is significantly higher than that of traditional NPUs, this capacity is still not sufficient to fit some of today’s DNN models that may be as big as several TBs (e.g., Transformer-1T [6]). Unfortunately, the exponential growth of the DNN model size only exacerbates the problem [39]. Thus, depending on the model size different execution modes are used as discussed next¹:

Weight Stationary. When models can be fit entirely on the available on-chip memory, loading the model and collecting

¹Note that in both execution modes, 3D parallelism can be used to distribute the training tasks across the NPUs.

the trained model to/from the wafer is a one-time overhead². The input samples, however, should be loaded at the beginning of the training iteration. Such I/O operations have little impact on the overall training performance. The cost of loading the model and storing the trained model is amortized over thousands of training iterations, and the input sample loading (usually much smaller than the model size) happens only at the beginning of the training iteration. In this case, the main performance factor is the efficiency of compute cores and the NPU-to-NPU communication performance. A non-optimized interconnect can result in **poor NPU-to-NPU communication performance** for certain parallelization strategies, forcing the compiler to discard some strategies, despite their better compute and on-chip memory utilization, only because of their poor communication performance (discussed later).

Weight Streaming. When the available on-chip memory is not enough to fit the model, the execution model changes to a method called *weight streaming* [1], [39]. Due to the lack of on-chip memory, the (one or a few) layers are loaded on the wafer, and when the processing of those layers is finished, the on-chip storage is reclaimed for the next set of layers. Therefore, in each training iteration the entire model needs to be loaded on-chip multiple times (at least once during the forward-pass, and once in the back-propagation). Another difference, compared to the previous case, is that when the cores compute the model gradients, they push it to the off-chip storage and a lightweight on-storage core is used to update the model for the next iteration³ [1]. This makes the performance to be I/O bound, meaning that the upper-bound training performance is $\propto \frac{\text{model_size}}{\text{I/O_BW}}$. Therefore, **in addition** to compute efficiency and NPU-to-NPU communication performance, maintaining the maximum I/O BW also plays a significant role in determining the overall performance. However, a rigid wafer-scale interconnect can create hotspots when distributing/collecting the model/gradients from/to the I/O channels. Such hotspots will **limit the I/O data rate** (discussed later) and directly hurt the training performance.

In summary, in both cases the wafer-scale interconnect plays a significant role in determining the training performance.

B. Desired Metrics

Next, we define desirable metrics to characterize different wafer-scale interconnect topologies for distributed training.

1) **Metric 1: Efficient I/O.**: As discussed earlier, maintaining high I/O BW is essential in achieving the best performance for the weight streaming execution model. However, baseline topologies like 2D-mesh fail to achieve the maximum I/O performance. Fig. 4 illustrates the problem on a 4×4 mesh topology with a pure DP parallelization strategy. Here, each weight fetched from an off-chip memory channel should be broadcast to all NPUs.

Fig. 4.a shows a broadcast algorithm, based on the *MPI* implementation of one-to-many pattern on mesh [2], when

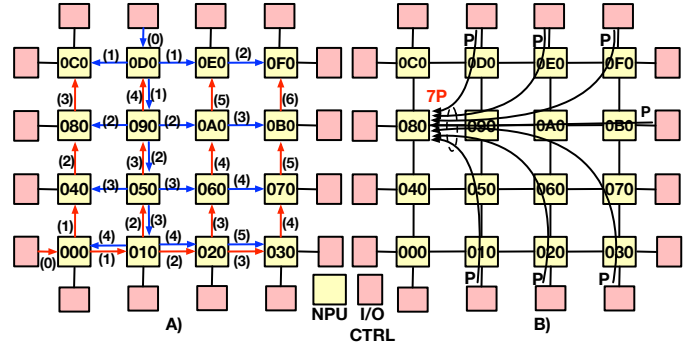


Fig. 4. (A) The broadcast communication pattern when reading from two different I/O channels (shown in red and blue arrows). The number associated with each arrow shows the timestamp when data crosses that link for one packet. In practice, multiple packets are pipelined across each path. In this example, the parallelization strategy is MP(1)-DP(16)-PP(1), and the model weights are broadcasted among all NPUs for the weight streaming execution model. Note that the reverse order is used to sum the weight gradients during the back-propagation and write the final results into the remote storage. (B) The maximum channel load analysis corresponding to Fig. 4.a, when all of the I/O channels are used simultaneously.

reading from two different memory channels (shown as the red and blue flows). Ideally, all memory channels should stream (different) weights simultaneously and with the line-rate to maximize the I/O BW. Fig. 4.b shows the maximum channel load analysis, for one hotspot link, when all memory channels are fetching the weights at the same time. If the BW of each memory channel is P bytes/s, then the hotspot link should have the capacity (BW) of $7P$ bytes/s to allow the maximum I/O BW on a 4×4 mesh.

In general, for an $N \times N$ mesh (and $4 \times N$ external I/O channels), the wafer-scale links should have the BW of $(2N - 1)P$ bytes/s to allow for the full I/O BW in all parallelization strategies, assuming each I/O channel BW is P bytes/s. As the formula shows, the required wafer-scale BW grows linearly with the mesh size and for certain mesh sizes, the technology may not allow providing such high-BW on wafer-scale. In this case, the I/O channel rate is scaled down proportional to the maximum BW of the wafer-scale links, i.e., $\frac{\text{link_BW}}{(2N-1)P}$.

FRED's solution: *FRED prevents such network hotspots by adaptively routing the traffic through all of its links equally, enabling for further scalability of the wafer-scale systems.*

2) **Metric 2: Ease of the Device Placement.**: Device placement determines the mapping of training workers to the physical NPUs. A system with N NPUs has $N!$ possible device placement mappings. Device placement becomes an important problem in 3D parallelism since each training worker might have different comm volumes/patterns with other workers (refer to Fig. 1). Hence, it is crucial to find a device placement with minimum network contention.

However, this is not a trivial task when dealing with rigid topologies like 2D-mesh where some of the comm patterns are prioritized over other patterns. Fig. 5 shows an example of two different mappings for a given MP(2)-DP(4)-PP(2) strategy. In Fig. 5.a, MP and DP comms are congestion-less but PP comms

²All model updates over different training iterations happen on-chip.

³Model update has a low operation intensity. Hence, updating the model off-chip prevents wasting the I/O BW to load the optimizer states on-chip for a light-weight operation.

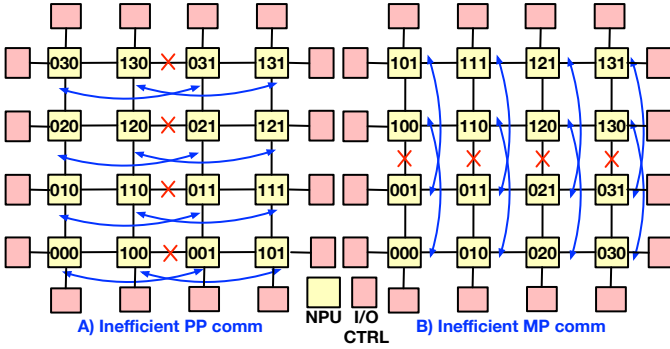


Fig. 5. Two different device placement mappings for an MP(2)-DP(4)-PP(2) strategy. (A) A device placement that favors MP and DP communications, but creates congestion for PP communication. (B) A device placement that favors DP and PP communications, but creates congestion for MP communication.

create congestion between different PP groups. In contrast, in Fig. 5.b, the DP and PP comms are optimized, while MP comms create congestion between MP groups.

As can be seen, device placement on 2D-mesh comes with two main challenges. First, due to the limited path diversity of 2D-mesh, some comm patterns should be prioritized over other patterns. Therefore, the non-optimized comms might add significant latency overhead to the training performance. Second, deciding which comm patterns to prioritize is challenging and requires careful analysis of the workload and identifying the overheads of different comm operations.

FRED’s solution: *FRED can support congestion-less routing of all communication patterns at the same time.*

3) **Metric 3: Non-Aligned Strategies.**: When searching for the best parallelization strategy, there are many possible configurations where the size of MP/DP/PP is not aligned with the physical topology dimensions. Such configurations create extra challenges on a 2D-mesh.

Fig. 6 shows an example of an MP(5)-DP(3)-PP(1) strategy on a 4×4 2D-mesh. Fig. 6.a shows how NPUs within the same MP group should communicate. Collective comms are usually optimized for well-structured topologies (e.g, ring, tree, switch, etc.). But as Fig. 6.a shows, each MP group forms a non-standard shape and it is not trivial what is the most optimized collective algorithm for each shape. This is contrary to FRED that has efficient collective algorithms for any size of MP/DP/PP. Fig. 6.b shows the extra traffic congestion introduced among two different DP groups, shown as red and blue, as a result of non-aligned dimensions. Although this strategy uses only two dimensions (PP=1), it still creates congestion on a 2D-mesh.

FRED’s solution: *FRED can handle congestion-less communications for any arbitrary size of MP/DP/PP.*

4) **Metric 4: Network BW Utilization.**: When dealing with the MP/DP/PP comms, it is hard or most of the times impossible to overlap all of these comms at the same time, since these comm operations are generated at different phases of the training algorithm. For example, MP comm is needed during both forward-pass/back-propagation and is a blocking operation, while DP comm happens during the back-

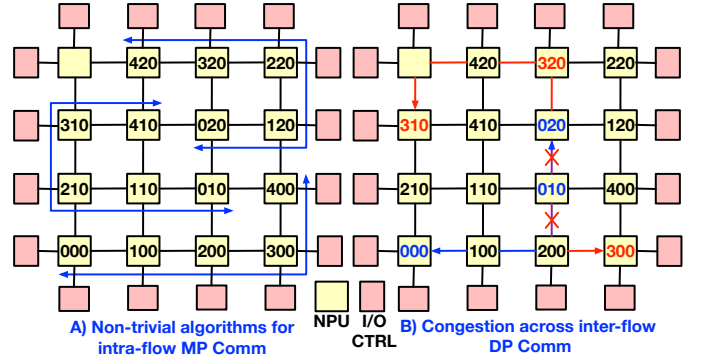


Fig. 6. Network comms on a 4×4 mesh topology for a non-aligned MP(5)-DP(3)-PP(1) parallelization strategy. (A) Non-optimized execution of comm patterns (e.g., All-Reduce) within the NPUs of the same MP group. (B) Traffic congestion between two different DP groups shown as red and blue assuming the X-Y routing (the traffic for other groups are not shown for clarity).

propagation only. Therefore, during the forward-pass, the links that are used for DP comm routing are not utilized. Therefore, maintaining the full BW utilization (during the communication operations) is not possible for many strategies on a 2D-mesh.

FRED’s solution: *FRED can utilize all of the NPU BW for each communication operation.*

5) **Metric 5: In-Network Collective Execution.**: As mentioned in Sec. II-B, supporting in-network collectives can significantly reduce the network traffic and improve the collective execution performance. Enabling in-network collectives requires centralized or hierarchical switches as a place to perform reductions/broadcast. Therefore, a 2D-mesh inherently cannot support in-network collectives.

FRED’s solution: *FRED utilizes a switch-based topology to support in-network collective execution.*

Takeaway. Overall, we would like to have a network interconnect that allows each NPU to drive its full network (injection) BW for any communication phase of 3D-parallel training without any congestion and with in-network collective support. Such properties cannot be supported using a 2D-Mesh network and are our main motivation for FRED.

IV. FRED NETWORK FABRIC ARCHITECTURE

FRED Switch. A FRED switch is the backbone of the FRED fabric. Hierarchical connections of the FRED switches form the full FRED fabric, which is explained in Sec. VI-A. The idea behind the FRED switch is simple: break the switch into the most fundamental components, and add small compute capability to each component. The fine-grained distribution of compute enables supporting flexible and concurrent in-switch collective execution for 3D parallelism communication patterns. In addition, distributed computation of collectives is more scalable for high BW of wafer-scale interconnects than having centralized compute and memory entities (see Sec. IX). Fig. 7(a) shows a FRED switch, which consists of a control unit, input port buffers, and the FRED interconnect. The control unit performs routing between the input ports and the output ports through the FRED interconnect.

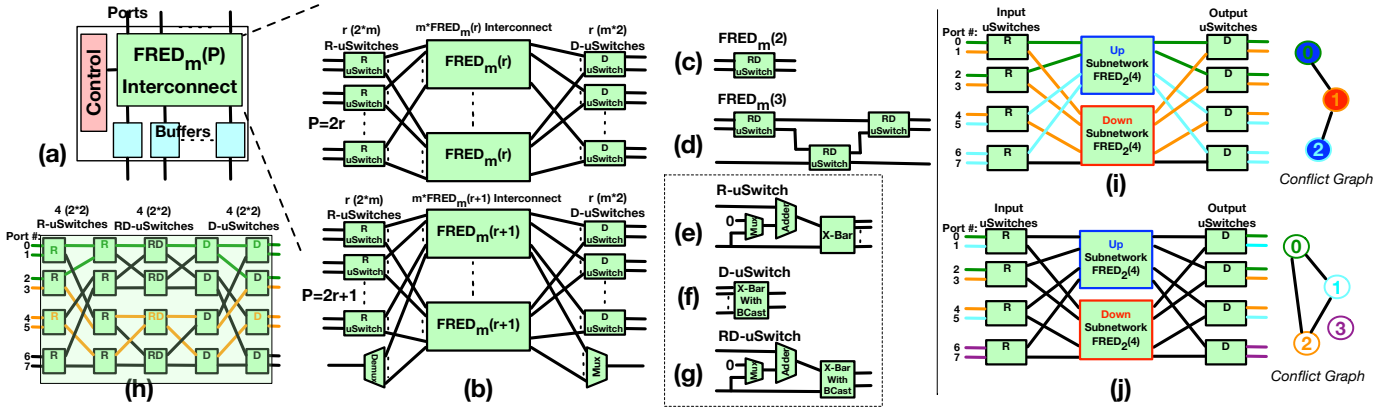


Fig. 7. (a) An overview of the FRED switch with P ports. (b) FRED interconnect (recursively constructed) when the number of ports are even ($2r$) or odd ($2r + 1$). (c) $FRED_m(2)$ switch. (d) $FRED_m(3)$ switch. (e) R - μ Switch. (f) D - μ Switch. (g) RD - μ Switch. (h) An example of a $FRED_2(8)$ interconnect implementation and two routed All-Reduce communication patterns (green and orange). (i) Routing Algorithm for three All-Reduce comm flows on $FRED_2(8)$ with conflict graph. (j) Example of Routing conflict.

FRED interconnect. The FRED interconnect, shown in Fig. 7(b), is inspired by *Clos* networks [14]. *Clos* networks are identified through the tuple (m, n, r) , where $m \geq 2$ is the number of middle stage switches, n is the number of input/output ports per each input/output micro-switch (μ Switch), and r is the number of input/output μ Switches. FRED’s connectivity is similar to the $(m, n = 2, r)$ *clos* network, which is denoted as $FRED_m(P)$. m denotes to the number of middle-stage switches, and P identifies the number of input(output) ports. FRED can be designed for an arbitrary number of ports by building on top of the previous works [12]. P is $2r/2r + 1$ when P is an even/odd number. Similar to the *Clos* network, FRED interconnect is constructed recursively, where the middle stage switches are the $m \times FRED_m(r)/m \times FRED_m(r+1)$ switches for the even/odd number of ports, as shown in Fig. 7(b). The recursive design of FRED ends when encountering to the base $FRED_m(2)$ or $FRED_m(3)$ Switches, which are depicted in Fig. 7(c) and Fig. 7(d) respectively.

FRED Microswitches. The main difference of FRED, compared to the baseline *Clos*, is adding the reduction and/or distribution (broadcast) support to the baseline μ Switches. This creates three types of μ Switches depending on which of these two features are present in the μ Switch. Fig. 7(e) shows the R - μ Switch structure that has the reduction feature, i.e., reducing data on the two input ports and routing to one of the output ports. Fig. 7(f) shows the D - μ Switch, that is able to perform distribution by broadcasting one of the input data to both output ports. RD - μ Switch is a 2×2 μ Switch and can perform both reduction and distribution, as shown in Fig. 7(g) The entire FRED switch is built using these three μ Switch types (plus *Muxes* and *Demuxes* to connect the last port to all intermediate stage switches when P is odd) through the recursive process explained earlier.

Example. Fig. 7(h) shows the complete structure of a $FRED_2(8)$ switch with two concurrent All-Reduce operations (green and orange). The highlighted $R/D/RD$ means that the

reduction / distribution / reduction-distribution features of the corresponding μ Switch are activated. For instance, the input μ Switch connecting the input ports 4, 5 performs the reduction and routes the result to one of its output ports. Other non-highlighted μ Switches operate like *Clos* μ Switches.

V. CONFLICT-FREE COLLECTIVE ROUTING

In this section, we discuss how different communication patterns are implemented over the FRED interconnect.

A. Communication Patterns on FRED

The fine-grained reduction and broadcast features enable FRED μ Switches to perform all different types of collective communication patterns observed in distributed training. Collective implementation on FRED however, can be abstracted through the notation of **communication flow** (or **flow** in short).

A *flow* on $FRED_m(P)$ includes a set of input ports (IPs)= $\{ip_1, ip_2, \dots, ip_i\}$ and output ports (OPs)= $\{op_1, op_2, \dots, op_j\}$, where $|IPs| \leq P$ and $|OPs| \leq P$. The *flow* results in reducing the data across the input ports determined in IPs and broadcasting the final result to the output ports identified in OPs . The port numbers and cardinality of IPs and OPs can be set independently, depending on the communication pattern. Each communication algorithm can be expressed in terms of performing one or more *flows*. For example, the orange All-Reduce pattern in Fig. 7(h) is a single *flow* with $IPs = \{3, 4, 5\}$ and $OPs = \{3, 4, 5\}$.

Simple Communication Algorithms. Simple communication algorithms refer to communication patterns that can be realized on FRED by performing only one *flow*. Table I summarizes different simple communication patterns on FRED and the number of involved input/output ports.

Compound Communication Algorithms. Compound communication algorithms realize the communication patterns through multiple *flows* on FRED. Table I summarizes different compound communication patterns on FRED. For example, *Reduce-Scatter* among i inputs are broken into i serial steps

of the *reduce flow*, and during step $1 \leq j \leq i$, the *reduce* operation corresponding the result of the op_j is done. The process is similar for other compound communication algorithms.

B. Routing Protocol

FRED considers a *flow* as a unit of routing, and supports concurrent routing of multiple *flows*. Similar to the previous methods [30], FRED routing protocol is also recursive, meaning that first the status of outermost μ Switch levels (i.e., input/output μ Switches) are determined, and then routing is recursively called on the middle stage switches. The difference is, however, supporting reduction/distribution features on the FRED μ switches, and the dependency between the input/output ports of a *flow*, which requires a new routing algorithm to realize these differences. FRED’s routing protocol is built upon the following intuitions:

- If two flows share the same input or output μ Switch, they should be routed through different middle-stage switches (subnetworks).
- If both input ports of an R- μ Switch or RD- μ Switch belong to the same *flow*, the reduction feature is activated.
- If both output ports of a D- μ Switch or RD- μ Switch belong to the same *flow*, the distribution (broadcast) feature of the μ Switch is activated.

The two latter points are easy to realize. To satisfy the first point, FRED routing protocol creates a *conflict graph*. Fig. 7(i) shows the first step of a routing example for a FRED₂(8) interconnect with the associated conflict graph for this step.

In the conflict graph, each node represents a *flow* and the edges between the nodes represent a conflict (i.e., sharing an input or output μ Switch) between the two nodes (*flows*). FRED routing applies the graph coloring on the conflict graph to find the routing of each *flow*. The number of colors is the number of intermediate stage switches (i.e., m). Fig. 7(i) also shows the results of the graph coloring. Here, there are only two colors since $m = 2$. Two flows are routed to the up subnetwork (blue), and one to the down subnetwork (red). After this step, the routing protocol and the conflict graph generation are recursively called on the middle blue and red FRED₂(4) switches. Note that a desired property of DL training is the deterministic and repetitive nature of its communication patterns that can be inferred at the compile time. Therefore, the routing algorithm for different comm phases of the training workload can be executed at the compile time and then saved at the control unit of the FRED switches and used during the training to minimize the routing overhead.

C. Routing Conflicts and Methods to Resolve

There are certain cases where not all *flows* can be routed at the same time, causing *routing conflict*. The routing conflict is identified when the graph coloring fails to color all of the nodes within the conflict graph. Fig. 7(j) shows an example of a routing conflict when there are four *flows* to be routed on a FRED₂(8) and the resulting conflict graph. The conflict graph cannot be colored using only two colors due to the circular dependencies between *flows*: 0, 1, 2. Note that the routing conflict may happen during any recursive call to the routing

TABLE I
SIMPLE (SHADED) AND COMPOUND COLLECTIVE ALGORITHMS.

Pattern	—IPs—	—OPs—	Comment
Unicast	1	1	
Multicast	1	>1	
Reduce	>1	1	
All-Reduce	$i > 1$	$i > 1$	Input ports and output ports are the same
Reduce-Scatter	$i > 1$	$i > 1$	Broken into multiple serial Reduce collectives, each on a different output port
All-Gather	$i > 1$	$i > 1$	Broken into multiple serial Multicast collectives, each on a different input port
Scatter	1	$i > 1$	Broken into multiple serial Unicast operations, each on a different output port
Gather	$i > 1$	1	Broken into multiple serial Unicast operations, each on a different input port
All-To-All	$i > 1$	$i > 1$	Broken into i serial steps of Unicast operations. In step $1 \leq j \leq i$, each input port unicasts to the output port with distance j in the OPs

algorithm (for routing the subnetworks). If the routing conflict is identified, the entire routing is marked to have conflict. We now discuss ways to address such conflicts.

(1) Blocking the Conflicting Flows. The first trivial way is to block some of the conflicting *flows* and run them after the other *flows* are finished. This translates to removing some of the nodes in the conflict graph. For e.g., in Fig. 7(j), if any of the *flows* 1, 2, or 3 is blocked, the routing can proceed to the next step (i.e., subnetworks). This option is, however, costly in terms of performance since it blocks some of the flows.

(2) Increasing the Number of Middle Stages. Another method is to design FRED switches with more intermediate stage switches (i.e., increase m). This method increases the number of colors for the graph coloring algorithm. Therefore, more conflicting *flows* can be routed simultaneously⁴. However, this comes at the expense of more HW overhead.

(3) Decomposing the Communication Algorithms. For the unicast-only traffic, FRED interconnect is *rearrangeably nonblocking* when $m = 2$, and *strict-sense nonblocking* when $m \geq 3$. This fact can be leveraged to decompose some of the communication algorithms into multiple steps and break the dependency among input/output ports in each step (i.e., making them unicast traffic). In the worst case, any collective algorithm can be decomposed into complete unicast traffic. For example, All-Reduce can be handled through a ring-based algorithm at the endpoints (NPUs), rather than in-network execution, which is a complete unicast traffic. As a result, *flows* 0, 1, and 2 in Fig. 7(j) can switch to ring-based All-Reduce at the endpoint, while *flow* 3 uses an in-network All-Reduce algorithm. This method solves the routing by degrading the communication performance of the conflicting *flows* (but it does not block any *flow*).

⁴For example, FRED₃(8) can route all the flows in Fig. 7(j).

TABLE II
PHYSICAL SYSTEM PARAMETERS

Component	Model	Area	Power	Characteristics
NPU Compute	GPU-like [9]	814 mm^2	525 W	<ul style="list-style-type: none"> FP16: 1,000 TFLOPS
NPU Memory	5 \times HBM3 [9], [32]	5 \times 100 mm^2	5 \times 35 W	<ul style="list-style-type: none"> Total Capacity: 80 GB Total BW: 3 TBps
Wafer-Scale Interconnect	SI-IF [32], [7]	4 μm pitch	0.063 pJ/bit Baseline: 100 W	<ul style="list-style-type: none"> # of Metal Layers: 2 Freq: 1.74 GHz BW: 53.7 GB/mm/metal layer BW/NPU Compute: 6 TBps/metal layer Latency: 20 ns
I/O Controller	CXL 3 [8]	18 \times 20 mm^2	18 \times 5 W	<ul style="list-style-type: none"> BW: 128 GBps/controller

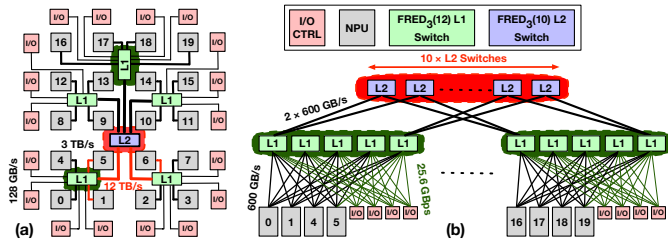


Fig. 8. Physical and Logical Views of 2-level FRED Topologies.

(4) **Intelligent Device Placement.** Another method to prevent conflicts is through intelligent device placement (mapping) of the training workers to the physical NPUs at the start time. For e.g., if in Fig. 7(j) the workers mapped to NPUs of port 1, 4 swap their locations, the conflict does not happen.

In *FRED* we prioritize the communication performance and do not use options (1) and (3). We use option (2) to simplify the device placement algorithm by only using $FRED_3(P)$ switches, ensuring that we have three colors in our routing algorithm protocol. Then, for the device placement algorithm, we map the training workers within the same MP group on consecutive physical NPUs followed by iterating over workers within PP and DP, respectively. This is sufficient to prevent routing conflicts for 3D-Parallelism communication patterns. Due to space limits, we do not show the full algorithm.

VI. WAFER SCALE ARCHITECTURE

A. Layout of FRED Fabric

A FRED switch builds a foundation to connect multiple wafer-scale NPUs. However, for large wafer-scale systems, due to physical limitations such as wiring, area, etc., it is not feasible to connect all of the NPUs through a single FRED switch. Hence, the *FRED fabric* provides a hierarchical design for the scalable connection of large wafer-scale systems. Fig. 8 shows an example of the FRED fabric that shows a 2-level tree connection of the FRED switches and the NPUs connected to the leaf (*L1*) Switches. In general, tree height and the BW across different levels are determined by the system size and physical constraints (see Sec. VI-B).

When there are multiple levels of FRED switches, the communication algorithms might need to cross several switches and hence, need to be optimized accordingly. For example, Fig. 8(a) shows the flow path for an All-Reduce between NPUs 1, 5, and 6. In this case, the data of NPUs 1 and 5 are reduced on their local L1 switch (to reduce the traffic going to the L2 switch), and the result along with the data of NPU 6 are reduced on the L2 switch. The final result is sent back to the corresponding L1 switches. The L1 switch attached to NPUs 1 and 5 also multicasts the result to the NPUs.

B. Wafer-scale Architecture Configuration

We assume a standard 300 mm wafer diameter, similar to the previous works [32], [7]. This results in 70000 mm^2 of wafer area. As previous works show, there are two physical limitations that limit the amount of compute and other resources on the wafer: (i) Thermal constraints, and (ii) power delivery network [31], [32], [7]. Thermal constraints limit

the amount of power that can be delivered to the wafer, depending on the cooling mechanism. Previous works report the maximum power limit within the 9.6 KW [32] to 15 kW [1] range. In this paper, we assume 15 kW power is available for the wafer-scale system. The other limitation is the power delivery network, which might necessitate using big on-wafer voltage regulator modules (VRMs), limiting the available area for NPUs [32]. However, alternative solutions can eliminate the need for on-wafer VRMs by either supplying the voltage from the top of the wafer [1], or delivering the power from the back of the wafer by using the *through-wafer-vias* (TWVs) [25]. In this paper, we assume the **on-wafer VRMs are not used** by using any of the solutions described earlier.

1) **Physical System Parameters:** Table II shows the other set of the physical parameters. We assume a GPU-like NPU compute chiplet each equipped with five stacks of HBM3 chiplet memories, resulting in combined power consumption of 700 W and area of 1314 mm^2 [9].

The NPU compute chiplet perimeter can support up to 12 TBps wafer-scale BW, where 6 TBps of it is allocated to support the 3 TBs local HBM memory BW (3 TBps for read + 3 TBps for write), and the other 6 TBps is allocated to support 3 TBps bi-directional total NPU-to-NPU BW (3 TBps for send + 3 TBps for receive).

The 15 KW power budget limits the total amount of NPUs on the wafer to 15 $KW/700 W \approx 21$, excluding other component power overheads (e.g., I/O controller, wafer-scale wires). In this paper we consider a 20-NPU wafer-scale system to make a room for other component power overheads. Additionally, 18 \times I/O Controllers are used to connect the wafer to the external memory. Hence, the total NPU + I/O Controller area overhead is 26640 mm^2 .

2) **Baseline Topology and Parameters:** The baseline topology is a 5 \times 4 2D-mesh with I/O controllers attached to the edge NPUs, similar to prior waferscale prototypes from Cerebras [1] and UCLA [32]. Each NPU-to-NPU link in the 2D-Mesh is equal to 750 GBps, resulting in the bisection BW of 3.75 TBps. The I/O Controller-to-NPU is 128 GBps.

TABLE III
HW OVERHEAD OF FRED IMPLEMENTATION OF FIG. 8(B).

Component	Area	Power
FRED ₃ (12) L1 Switch	15 × 685 mm ²	15 × 2.73 W
FRED ₃ (11) L1 Switch	10 × 678 mm ²	10 × 2.50 W
FRED ₃ (10) L2 Switch	10 × 814 mm ²	10 × 2.28 W
Additional Wafer-Scale Wiring	N/A	58 W
Total	25195 mm ²	146.73 W

3) **FRED Topology and Parameters:** To motivate FRED, we leverage the fact that the combination of a constrained power budget and high-end NPUs results in utilizing 26640 mm² out of 70000 mm² area overhead, **making room to utilize otherwise unclaimed area for more efficient interconnects like FRED.** However, FRED or any other proposal must have low power consumption since most power budget is allocated to the NPUs. Here, **we demonstrate that FRED meets these properties.**

Our target FRED topology is similar to Fig. 8(a), where 20 NPUs and I/O controllers are connected through a 2-level (almost) fat-tree topology. Similar to the baseline, the BW/NPU is still 3 TBps, but the bisection BW is increased to 30 TBps. It is almost fat-tree since the L1-to-L2 BW is the summation of attached NPU BW only (and not NPU + I/O Controller). The reason is that if one participant of any *flow* (e.g., *Reduce*) is an I/O controller, then the entire *flow's* BW requirement is determined by the I/O controller's BW (e.g., 128 GBps), which is significantly less than NPU-to-NPU BW. Hence, an almost fat-tree gives the same performance as the full fat-tree.

Looking at the BW requirements of FRED L1/L2 switches in Fig. 8(a), it is clear that each switch chiplet requires a perimeter, to connect the wafer-scale network wires, that is not feasible to build. Hence, in reality each of the FRED switches in Fig. 8(a) is decomposed into multiple lower-BW FRED chiplets. Fig. 8(b) shows a logical view of implementing the (almost) fat-tree based topology of Fig. 8(a) using feasible FRED chiplets. As Fig. 8(b) shows, each switch of Fig. 8(a) is implemented by decomposing it into multiple smaller, but feasible, FRED switches (enclosed in the strip line). For our evaluations, we use FRED₃(*P*) switches.

HW Overhead. Table III shows the overheads of our proposed FRED (with 24 KB/port buffer size and 1KB buffer to store the routings in the control unit) implementation shown in Fig. 8. The numbers are obtained post layout using 15nm NanGate PDK. The total power overhead is 146.73 W, which is less than 1 % of the total power budget. The total area overhead is 25195 mm² which can be accommodated by using the unclaimed area available on the wafer. Note that, as discussed in Sec. VI-B3, the main area overhead of the FRED chiplets is due to I/O for supporting high-BW wafer-scale interconnects, and not because of the switch logic overhead.

VII. EVALUATION METHODOLOGY

A. FRED Configurations

We test four different variations of FRED to show how different features of FRED contribute to the overall performance. Table IV shows the target configurations. *FRED-A* shows the

TABLE IV
TARGET CONFIGURATIONS.

Configs	Comment
Baseline	The baseline topology where 20 NPUs are formed using a 4×5 2D-mesh topology (3.75 TBps bisection). Each border NPU is attached to an I/O controller, except for the corner NPUs that are connected to two I/O controllers, summing the total I/O controllers to 18.
FRED-A	FRED topology where 20 NPUs and 18 I/O controllers are connected similar to Fig. 8, but with the same bisection BW as the baseline (3.75 TBps) . This is achieved by downscaling L1-L2 links from 12 TBps, in Fig. 8(a), to 1.5 TBps. Additionally, it does not support in-switch collective execution . Thus, collective algorithms are handled at the endpoints.
FRED-B	Similar to FRED-A, but with in-network collective execution .
FRED-C	FRED topology where 20 NPUs and 18 I/O controllers are connected similar to Fig. 8 (30 TBps bisection), but without any in-switch collective execution (handled at the endpoint).
FRED-D	Similar to FRED-C, but with in-network collective execution .

TABLE V
TARGET WORKLOADS

Workload	Parallelization Strategy	Execution Model
ResNet-152 [15]	MP(1)_DP(20)_PP(1)	<i>Weight Stationary</i>
Transformer-17B [5]	MP(3)_DP(3)_PP(2)	<i>Weight Stationary</i>
GPT-3 [11]	MP(2)_DP(5)_PP(2)	<i>Weight Streaming</i>
Transformer-1T [6]	MP(1)_DP(20)_PP(1)	<i>Weight Streaming</i>

effect of going from mesh to switch-based topology with the same bisection and without in-network collective execution. *FRED-B* builds on top of FRED-A and adds the in-network collective execution feature. *FRED-C* increases the bisection BW without in-network collective execution. Finally, FRED-D is the most optimal variant of FRED by adding the in-network collective execution to the previous variant.

B. Collective Algorithm

For the baseline 2D mesh and when there is a wafer-wide collective, we use the hierarchical 2D algorithm with 2 concurrent chunks (in reverse direction) as explained in [19]. For collectives between arbitrary NPUs, we build logical rings between involved NPUs and perform the ring algorithm. We also use the X-Y routing which is common in real systems [19]. For FRED-A and FRED-C, we use the hierarchical 2-D ring algorithm to reduce the traffic of L1-L2 links, similar to [13]. FRED-B and FRED-D use the in-network capability and use the hierarchical FRED switch topology to perform the collective, as explained in Sec. VI-A.

C. Target Workloads and Execution modes

Table V shows the target workloads and their corresponding parallelization strategy and execution models. ResNet-152 and Transformer-17B (Transformer model with 17 billion parameters) can fit on the on-wafer memory and hence, use the *weight stationary* execution mode (Sec. III-A). In contrast, GPT-3 and Transformer-1T (Transformer model with 1 trillion parameters) use the *weight streaming* execution mode (Sec. III-A). Workers within the same DP group perform All-Reduce together during the back-propagation to sync on weigh

gradients. Note that in *weight streaming* mode, the DP groups should reduce the gradients as they stream them out to the external memory through the I/O controller. The pattern is reverse communication direction of Fig. 4.

For both Transformer-17B and GPT-3, the model split is based on the Megatron-LM method [41], which requires two All-Reduces (along the MP dimension) for each transformer layer stack during fwd-pass & back-propagation. For the PP split on Transformer-17B, we assume the minibatch is divided into 8 microbatches to hide the effect of pipeline bubbles [16]. For GPT-3, however, pipelining works differently since it is combined with the weight streaming. In this case, $PP = 2$ indicates that each time 2 consecutive layers are brought to the wafer and distributed among different NPUs along the PP dimension. Thus, splitting the minibatch into two microbatches is enough to hide the pipeline latency.

We assume the device placement strategy for the baseline favors MP, PP, and DP in the descending order of priority, similar to the previous works [28]. We also assume the gradient, activation, and model parameters have the FP16 type. The minibatch size for all workloads is $DP_size \times 16$.

We note that our choice of workload parallelization strategies is not claimed to be the optimal strategy on the baseline or FRED platform. The purpose of this paper is to show the efficiency and flexibility of FRED, compared to the baseline topology, for all different parallelization strategies. Further co-optimizing of the parallelization strategy with the underlying platform (baseline or FRED) is beyond the scope of this paper, and is the subject of our future work.

D. Simulation Framework

We use ASTRA-SIM [35], [3], which is an open-source simulation methodology for modeling distributed training systems. ASTRA-SIM can model various parallelization strategies and the overlapping of compute with comm kernels. Additionally, its network back-end can simulate the comm operations in detail. We extend ASTRA-SIM to model the I/O-to-wafer transfers for both the weight stationary and weight streaming scenarios. For each workload, we run the simulation for two training iterations (i.e., two forward + two backward-pass).

Metric of Evaluation. In Sec. VIII, we report the end-to-end training times and their breakdowns into total compute time and different *exposed* communication times. The exposed communication time refers to the amount of time that is not overlapped with the compute time and the workload is waiting for the communication to be finished. Depending on the parallelization strategy and execution model, there might be multiple sources of exposed communication times - due to load, DP, MP, PP, and/or weight streaming.

VIII. RESULTS

Microbenchmark Results. Fig. 9 presents the communication breakdown across 3D parallelism phases for two parallelization strategies for Transformer-17B.

For the MP(20)-DP(1)-PP(1) strategy, there are only wafer-wide All-Reduce operations for the MP communication. The baseline effective BW utilization is bounded by the corner

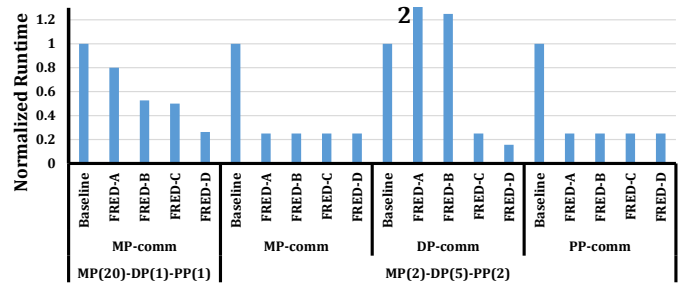


Fig. 9. Communication microbenchmark results for comparing only comm performance at different phases of 3D-parallelism, for two different parallelization strategies of Transformer-17B from Fig. 2.

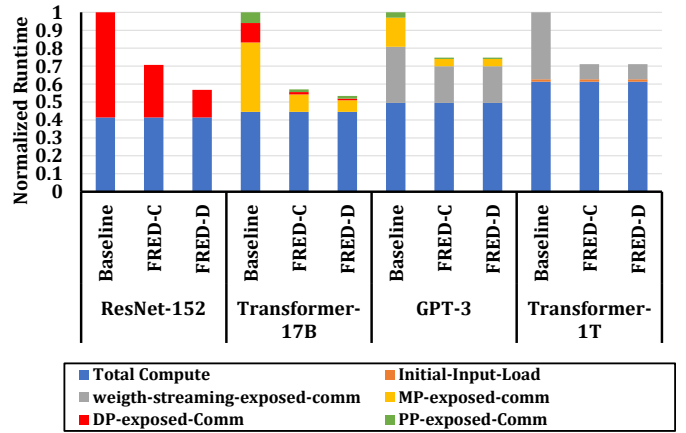


Fig. 10. End-to-end training times decomposed into compute times and different communication times. The runtime of each workload is normalized to its corresponding baseline.

NPUs since they have only 2 links to other NPUs. This limits the average network BW utilization of each NPU to be around $2 \times 750GBps = 1500GBps$. In FRED-A, each NPU-L1 BW is 3 TBps, but NPU-L2 BW is 375 GBps.⁵ Using a similar analysis as [36], we see that hierarchical collectives result in NPU-L2 BW being the bottleneck and the effective NPU BW utilization is $375GBps + 4 \times 375GBps = 1850GBps$. In FRED-B, the L1 switches first perform the All-Reduce and then use the entire L1-L2 BW to forward the data to the L2 switches for the second All-Reduce. Therefore, each NPU can send the data to L2 switch at the speed of 1500GBps (L1-L2 BW). However, since it is an in-network collective execution, the amount of traffic each NPU sends out is almost half of the traffic in the endpoint-based collective. FRED-C has much more L1-L2 BW and therefore each NPU can drive the BW utilization to 3 TBps. In FRED-D, an additional in-network collective execution reduces the traffic by half in addition to the 3 TBps NPU BW utilization.

The MP(2)-DP(5)-PP(2) case has all MP (All-Reduce), DP (All-Reduce) and PP (multicast) comms. For the MP comms, the baseline NPU can only utilize 1 link (out of its up to 4 links), resulting in only 750 GBps BW utilization. Since all the communicating NPUs are below the same L1 switch in FRED topologies, they can use the entire 3 TBps of NPU-L1 BW to communicate. Additionally, in the special case when

⁵Assuming the L1-L2 BW is equally shared among all NPUs.

the number of peer NPUs is two, the amount of traffic for endpoint-based vs. in-network execution is the same. Hence, all FRED variants have the same performance for MP comm.

For DP comm, again the baseline is limited by the corner NPUs which can utilize only 1 of their links for DP comm. Hence the baseline NPU BW is 750 GBps. In FRED, and for the DP comm, each NPU should communicate with four other NPUs under different L1 switches. Therefore, in FRED variants the L1-L2 BW should be shared across four collective flows. Therefore, L1-L2 BW plays a significant role in the performance of this collective. In FRED-A, each NPU has an average NPU-L2 BW of 375 GBps, and hence, the NPU BW utilization is only 375 GBps, which is worse than the baseline. In FRED-B, however, the L2 switch is used to perform All-Reduce for each flow. This reduces the traffic generated by each NPU roughly by 37.5%, which makes its overall performance closer to the baseline. In FRED-C, however, the NPU-L2 BW is increased to 3 TBps. Finally, FRED-D improves the FRED-C by performing in-network collective execution and reducing the traffic by 37.5%.

For the PP comm, the baseline NPU can utilize one of its links to forward data to the next pipeline stage and hence, its BW utilization is 750GBps. Note that this is possible since in the case of language models such as Transformer-17B, one NPU within the mp group is sufficient to multicast the output to all NPUs at the next stage⁶, and hence, there is no contention between NPUs of the same mp group at the same stage. In FRED, all peer NPUs are below the same L1 switch and can utilize the entire 3TBps BW for the PP comm.

Full Workload Results. Fig. 10 shows the end-to-end runtimes of the training workloads for the baseline vs. FRED. Due to space limitation, we only show the FRED-C and FRED-D in comparison with the baseline. In general, input activations, compared to the model parameters, are relatively small in size and hence, do not have significant overhead on the total iteration time. Additionally, the input activations of the next iteration can be prefetched to the wafer whenever the wafer-scale interconnect is idle. Hence, we observe **no initial_input_load** exposed comm for any of our target workloads, except for the Transformer-1T that is explained later.

ResNet-152 uses pure DP with a weight stationary model. Hence, the only communication costs repeating on each training iteration are the input minibatch loading and DP communication. As explained earlier, in wafer-wide All-Reduce collective, the baseline is able to utilize 1.5 TBps of NPU BW. FRED-C and FRED-D can achieve 3 TBps NPU BW but FRED-D can further reduce the network traffic by $\approx 2\times$. This results in a significant reduction of DP exposed comm. Thus, FRED-C and FRED-D can improve the end-to-end training runtime by 1.41 \times and 1.76 \times , respectively for ResNet-152.

Transformer-17B uses all dimensions of the 3D-parallelism and therefore, has all DP, MP, and PP communication overheads. The baseline device placement favors MP, but compromises the PP and DP comms, especially due to the non-aligned

parallelization strategy dimensions as explained in Sec. III. Another drawback of the baseline is the underutilized links due to the non-overlapping nature of MP/DP/PP comms (see section Sec. III). FRED-C, on the other hand, does not have the problem of underutilized links and non-aligned parallelization strategies. It also does not require to favor any of DP, MP, or PP over the other strategies. FRED-D can further improve the MP and DP collective performance due to in-switch collective execution capability. As a result, FRED-C can improve the overall end-to-end training performance by 1.75 \times and 1.87 \times , respectively.

GPT-3 combines weight streaming with 3D-parallelism. Using the analysis of Sec. III, the baseline topology is unable to stream weights with the full line-rate of I/O controllers. The reason is that, the hotspot link requires $(2 \times 5 - 1) \times 128$ GBps = 1152 GBps, while link capacity is only 750 GBps. Therefore, the I/O channels should work with $\frac{750}{1152} = 0.65\times$ of the line-rate. The MP/PP comm performance of FRED-C and FRED-D's is $\approx 4\times$ better than the baseline, due to the underutilized links in the baseline. Note that the reason why FRED-C and FRED-D have the same performance for MP collective comm is because $\dim(\text{MP})=2$. In this special case, as explained earlier, end-to-end and in-switch collective execution have the same amount of networking traffic and hence, have the same performance. In total FRED-D and FRED-C outperform the baseline by 1.34 \times in terms of overall training time for GPT-3.

Transformer-1T is another weight streaming workload but with only DP parallelism. As a result, the weight streaming delay is the only comm overhead in addition to the initial input load. The high-performance compute NPUs and limited off-chip I/O BW puts the weight streaming performance directly on the critical path. This means that the NPUs can work with the line-rate of the weight being streamed, and the main limiting factor is how fast all the weights can be streamed. In this case, both FRED-C and FRED-D can leverage the full I/O BW, while the baseline topology can only work with 0.65 \times of the total I/O BW as explained earlier. Additionally, since I/O controllers are always being utilized for weight streaming, there is no idle time to prefetch the input minibatch of the next iteration during the current training iteration. Hence, the initial input load cannot be hidden, although its overhead is very negligible. In total, using FRED-C/FRED-D improves the training time of Transformer-1T by 1.4 \times .

IX. RELATED WORKS

FRED is the first wafer-scale interconnect fabric optimized for distributed training. However, the idea of in-switch collective execution has been proposed in many previous works for different network levels which we discuss next. *P4* language [10] allows for offloading the application-specific tasks to the network switches that support P4 abstract architecture. [37], [20] proposed programming the datacenter ethernet switches for offloading the All-Reduce collective for data-parallel training strategies. iSwitch [24] utilizes FPGA logic within switches to offload the All-Reduce functionality for the distributed training of reinforcement learning. Mellanox

⁶All NPUs within the same MP group produce the same output in this case

SHARP [4] is an Infiniband switch architecture for performing the collectives. Authors in [18] proposed a method to offload collectives to the scale-up NPU fabric (e.g., [22]).

A fundamental difference between these works and FRED is that they are proposed for off-chip networks which have significantly less BW compared to the on-chip wafer-scale networks. In many of these solutions, the internal switch BW should be at least $2\times$ and $P\times$ of the link BW to be efficient (i.e., line-rate) for All-Reduce and Reduce between P ports, respectively. The reason is because of the switch architecture that performs the reductions only after the routing and on the output port. While the difference between the off-chip links and on-chip switch architectures allows for provisioning such BW difference, it is not applicable for wafer-scale platforms where the links are on-chip and can have the same BW as the switches. In contrast, FRED performs the reduction operations in multiple steps (μ Switches) during the routing on the FRED interconnect. Hence the FRED switch works with the same BW of the links and can provide line-rate throughput.

X. CONCLUSION

We propose FRED, a high-BW wafer-scale interconnect and fabric that is flexible for different configurations of the 3D parallelization strategies of distributed training workloads. FRED is able to support concurrent in-network collective execution efficiently, enabling the upper-level compiler to further optimize the parallelization strategy for compute and memory utilization. This work opens up several research opportunities for parallelism and wafer-scale fabric co-design.

REFERENCES

- [1] "Cerebras Systems: Achieving Industry Best AI Performance Through A Systems Approach," <https://f.hubspotusercontent30.net/hubfs/8968533/Cerebras-CS-2-Whitepaper.pdf>.
- [2] "MPI: A Message-Passing Interface Standard," <https://www.mpi-forum.org/docs/mpi-3.1/mpi31-report.pdf>, 2015.
- [3] "ASTRA-SIM: Enabling SW/HW Co-Design Exploration for Distributed DL Training Platforms," <https://github.com/astra-sim/astra-sim.git>, 2020.
- [4] "Mellanox SHARP," <https://docs.mellanox.com/display/sharpv214>, 2020.
- [5] "Turing-NLG: A 17-billion-parameter language model by Microsoft," <https://www.microsoft.com/en-us/research/blog/turing-nlg-a-17-billion-parameter-language-model-by-microsoft/>, 2020.
- [6] "Google Open-Sources Trillion-Parameter AI Language Model Switch Transformer," <https://www.infoq.com/news/2021/02/google-trillion-parameter-ai/>, 2021.
- [7] "Scale-Out Packageless Processing," <https://nanocad.ee.ucla.edu/wp-content/papercite-data/pdf/phdth11.pdf>, 2021.
- [8] "Compute Express Link 3.0," https://www.computeexpresslink.org/_files/ugd/0c1418_a8713008916044ae9604405d10a7773b.pdf, 2022.
- [9] "NVIDIA H100 Tensor Core GPU," <https://www.nvidia.com/en-us/data-center/h100/>, 2022.
- [10] P. Bosshart, D. Daly, G. Gibb, M. Izzard, N. McKeown, J. Rexford, C. Schlesinger, D. Talayco, A. Vahdat, G. Varghese, and D. Walker, "P4: Programming protocol-independent packet processors," *SIGCOMM Comput. Commun. Rev.*, vol. 44, no. 3, p. 87–95, jul 2014. [Online]. Available: <https://doi.org/10.1145/2656877.2656890>
- [11] T. B. Brown, B. Mann, N. Ryder, M. Subbiah, J. Kaplan, P. Dhariwal, A. Neelakantan, P. Shyam, G. Sastry, A. Askell, S. Agarwal, A. Herbert-Voss, G. Krueger, T. Henighan, R. Child, A. Ramesh, D. M. Ziegler, J. Wu, C. Winter, C. Hesse, M. Chen, E. Sigler, M. Litwin, S. Gray, B. Chess, J. Clark, C. Berner, S. McCandlish, A. Radford, I. Sutskever, and D. Amodei, "Language models are few-shot learners," 2020.
- [12] C. Chang and R. Melhem, "Arbitrary size benes networks," *Parallel Processing Letters*, vol. 07, no. 03, pp. 279–284, 1997. [Online]. Available: <https://doi.org/10.1142/S0129626497000292>
- [13] M. Cho, U. Finkler, M. Serrano, D. Kung, and H. Hunter, "Blueconnect: Decomposing all-reduce for deep learning on heterogeneous network hierarchy," *IBM Journal of Research and Development*, vol. 63, no. 6, pp. 1:1–11, Oct. 2019.
- [14] C. Clos, "A study of non-blocking switching networks," *Bell System Technical Journal*, vol. 32, no. 2, pp. 406–424, 1953.
- [15] K. He, X. Zhang, S. Ren, and J. Sun, "Deep residual learning for image recognition," 2015.
- [16] Y. Huang, Y. Cheng, A. Bapna, O. Firat, M. X. Chen, D. Chen, H. Lee, J. Ngiam, Q. V. Le, Y. Wu, and Z. Chen, "Gpipe: Efficient training of giant neural networks using pipeline parallelism," 2018. [Online]. Available: <https://arxiv.org/abs/1811.06965>
- [17] Z. Jia, M. Zaharia, and A. Aiken, "Beyond data and model parallelism for deep neural networks," *CoRR*, vol. abs/1807.05358, 2018. [Online]. Available: <http://arxiv.org/abs/1807.05358>
- [18] B. Klenk, N. Jiang, G. Thorson, and L. Dennison, "An in-network architecture for accelerating shared-memory multiprocessor collectives," in *47th Annual International Symposium on Computer Architecture*, ser. ISCA, 2020, pp. 996–1009.
- [19] S. Kumar and N. Jouppi, "Highly available data parallel ml training on mesh networks," 2020. [Online]. Available: <https://arxiv.org/abs/2011.03605>
- [20] C. Lao, Y. Le, K. Mahajan, Y. Chen, W. Wu, A. Akella, and M. Swift, "ATP: In-network aggregation for multi-tenant learning," in *18th USENIX Symposium on Networked Systems Design and Implementation (NSDI 21)*. USENIX Association, Apr. 2021, pp. 741–761. [Online]. Available: <https://www.usenix.org/conference/nsdi21/presentation/lao>
- [21] D. Lepikhin, H. Lee, Y. Xu, D. Chen, O. Firat, Y. Huang, M. Krikun, N. Shazeer, and Z. Chen, "Gshard: Scaling giant models with conditional computation and automatic sharding," 2020. [Online]. Available: <https://arxiv.org/abs/2006.16668>
- [22] A. Li, S. L. Song, J. Chen, J. Li, X. Liu, N. R. Tallent, and K. J. Barker, "Evaluating modern GPU interconnect: Pcie, nvlink, nv-sli, nvswitch and gpudirect," 2019.
- [23] S. Li, Y. Zhao, R. Varma, O. Salpekar, P. Noordhuis, T. Li, A. Paszke, J. Smith, B. Vaughan, P. Damania, and S. Chintala, "Pytorch distributed: Experiences on accelerating data parallel training," 2020. [Online]. Available: <https://arxiv.org/abs/2006.15704>
- [24] Y. Li, I.-J. Liu, Y. Yuan, D. Chen, A. Schwing, and J. Huang, "Accelerating distributed reinforcement learning with in-switch computing," in *46th International Symposium on Computer Architecture*, ser. ISCA, 2019, p. 279–291. [Online]. Available: <https://doi.org/10.1145/3307650.3322259>
- [25] M.-H. Liu, B. Vaisband, A. Hanna, Y. Luo, Z. Wan, and S. S. Iyer, "Process development of power delivery through wafer vias for silicon interconnect fabric," in *2019 IEEE 69th Electronic Components and Technology Conference (ECTC)*, 2019, pp. 579–586.
- [26] T. P. Morgan, "Inside Tesla's Innovative and Homegrown 'Dojo' AI Supercomputer," <https://www.nextplatform.com/2022/08/23/inside-teslas-innovative-and-homegrown-dojo-ai-supercomputer/>, 2022.
- [27] D. Narayanan, A. Harlap, A. Phanishayee, V. Seshadri, N. R. Devanur, G. R. Ganger, P. B. Gibbons, and M. Zaharia, "Pipedream: Generalized pipeline parallelism for dnn training," ser. SOSP '19. New York, NY, USA: Association for Computing Machinery, 2019, p. 1–15. [Online]. Available: <https://doi.org/10.1145/3341301.3359646>
- [28] D. Narayanan, M. Shoeybi, J. Casper, P. LeGresley, M. Patwary, V. Korthikanti, D. Vainbrand, P. Kashinkunti, J. Bernauer, B. Catanzaro, A. Phanishayee, and M. Zaharia, "Efficient large-scale language model training on gpu clusters using megatron-lm," in *Proceedings of the International Conference for High Performance Computing, Networking, Storage and Analysis*, ser. SC '21. New York, NY, USA: Association for Computing Machinery, 2021. [Online]. Available: <https://doi.org/10.1145/3458817.3476209>
- [29] M. Naumov, D. Mudigere, H. M. Shi, J. Huang, N. Sundaraman, J. Park, X. Wang, U. Gupta, C. Wu, A. G. Azzolini, D. Dzhalgakov, A. Malle- vich, I. Cherniavskii, Y. Lu, R. Krishnamoorthi, A. Yu, V. Kondratenko, S. Pereira, X. Chen, W. Chen, V. Rao, B. Jia, L. Xiong, and M. Smelyanskiy, "Deep learning recommendation model for personalization and recommendation systems," 2019.

- [30] D. Nikolaidis, P. Groumas, C. Kouloumentas, and H. Avramopoulos, "Novel benes network routing algorithm and hardware implementation," *Technologies*, vol. 10, no. 1, 2022. [Online]. Available: <https://www.mdpi.com/2227-7080/10/1/16>
- [31] S. Pal, J. Liu, I. Alam, N. Cebry, H. Suhail, S. Bu, S. S. Iyer, S. Pamarti, R. Kumar, and P. Gupta, "Designing a 2048-chiplet, 14336-core waferscale processor," in *2021 58th ACM/IEEE Design Automation Conference (DAC)*, 2021, pp. 1183–1188.
- [32] S. Pal, D. Petrisko, M. Tomei, P. Gupta, S. S. Iyer, and R. Kumar, "Architecting waferscale processors - a gpu case study," in *2019 IEEE International Symposium on High Performance Computer Architecture (HPCA)*, 2019, pp. 250–263.
- [33] D. Patel, "Tenstorrent Wormhole Analysis - A Scale Out Architecture for Machine Learning That Could Put Nvidia On Their Back Foot," <https://www.semianalysis.com/p/tenstorrent-wormhole-analysis-a-scale/>, 2022.
- [34] S. Rashidi, P. Shurpali, S. Sridharan, N. Hassani, D. Mudigere, K. Nair, M. Smelyanski, and T. Krishna, "Scalable distributed training of recommendation models: An astra-sim + ns3 case-study with tcp/ip transport," in *2020 IEEE Symposium on High-Performance Interconnects*, ser. HOTI, 2020, pp. 33–42.
- [35] S. Rashidi, S. Sridharan, S. Srinivasan, and T. Krishna, "Astra-sim: Enabling sw/hw co-design exploration for distributed dl training platforms," in *2020 IEEE International Symposium on Performance Analysis of Systems and Software*, ser. ISPASS, 2020, pp. 81–92.
- [36] S. Rashidi, W. Won, S. Srinivasan, S. Sridharan, and T. Krishna, "Themis: A network bandwidth-aware collective scheduling policy for distributed training of dl models," in *Proceedings of the 49th Annual International Symposium on Computer Architecture*, ser. ISCA '22. New York, NY, USA: Association for Computing Machinery, 2022, p. 581–596. [Online]. Available: <https://doi.org/10.1145/3470496.3527382>
- [37] A. Sapio, M. Canini, C.-Y. Ho, J. Nelson, P. Kalnis, C. Kim, A. Krishnamurthy, M. Moshref, D. Ports, and P. Richtarik, "Scaling distributed machine learning with In-Network aggregation," in *18th USENIX Symposium on Networked Systems Design and Implementation (NSDI 21)*. USENIX Association, Apr. 2021, pp. 785–808. [Online]. Available: <https://www.usenix.org/conference/nsdi21/presentation/sapio>
- [38] J. Schemmel, D. Brüderle, A. Grübl, M. Hock, K. Meier, and S. Millner, "A wafer-scale neuromorphic hardware system for large-scale neural modeling," in *2010 IEEE International Symposium on Circuits and Systems (ISCAS)*, 2010, pp. 1947–1950.
- [39] Sean Lie, "Thinking Outside the Die: Architecting the ML Accelerator of the Future," <https://www.microarch.org/micro54/media/lie-keynote.pdf>, 2021.
- [40] Y. S. Shao, J. Clemons, R. Venkatesan, B. Zimmer, M. Fojtik, N. Jiang, B. Keller, A. Klinefelter, N. Pinckney, P. Raina, S. G. Tell, Y. Zhang, W. J. Dally, J. Emer, C. T. Gray, B. Khailany, and S. W. Keckler, "Simba: Scaling deep-learning inference with multi-chip-module-based architecture," in *52nd Annual IEEE/ACM International Symposium on Microarchitecture*, ser. MICRO, 2019, p. 14–27. [Online]. Available: <https://doi.org/10.1145/3352460.3358302>
- [41] M. Shoeybi, M. Patwary, R. Puri, P. LeGresley, J. Casper, and B. Catanzaro, "Megatron-lm: Training multi-billion parameter language models using model parallelism," 2020.
- [42] R. Thakur, R. Rabenseifner, and W. Gropp, "Optimization of collective communication operations in mpich," *International Journal of High Performance Computing Applications*, vol. 19, no. 1, pp. 49–66, Feb. 2005. [Online]. Available: <http://dx.doi.org/10.1177/1094342005051521>